



Porosity estimation and pore structure characterization of foamed cement paste using non-specialized image digital processing

Lina Chica · Carlos Mera · Lina María Sepúlveda-Cano · Albert Alzate

Received: 23 March 2022 / Accepted: 10 August 2022 / Published online: 25 August 2022
© The Author(s) 2022

Abstract In foamed concrete, porosity is essential because it is strongly related to other properties such as density, permeability, and strength. Porosity measurement (usually expressed as a percentage of total volume) is obtained in a laboratory using experimental water vacuum saturation and MIP methods. However, pore structure -including size, distribution, shape, and connection- is also needed to understand foamed concrete performance. Pore structure characterization is estimated through specialized digital image analysis. Micro CT, scanning electron microscopy or X-ray tomography images are frequently used to obtain pore

structure on cellular concrete. However, these images are highly specialized and require equipment that is not easy to find and very expensive. Also, image processing is complex, and it includes some specialized software. This paper presents a pore structure characterization and porosity estimation using non-specialized digital images on foamed cement paste made with alternative agents. The procedure for acquiring images uses only a camera without any specialized equipment. The proposed methodology isolates the pores in the image and measures shape features such as pore diameter, eccentricity, and solidity. Acquiring and processing the images is simpler, faster, and cheaper than other specialized analyses. Results show that the volumetric porosity estimation was entirely accurate, with an estimation deviation of less than 10%. Also, the pore structure parameters such as pore size and distribution of foamed pastes can be quantified accurately.

Carlos Mera, Lina María Sepúlveda-Cano and Albert Alzate were contributed equally to this work.

L. Chica (✉) · A. Alzate
Facultad de Ingenierías, Universidad de Medellín, Carrera 87 30-65, Medellín 050023, Antioquia, Colombia
e-mail: lmchica@udemedellin.edu.co

A. Alzate
e-mail: alalzate@udemedellin.edu.co

C. Mera
Facultad de Ingenierías, Instituto Tecnológico Metropolitano - ITM, Carrera 54A 30-01, Medellín 050023, Antioquia, Colombia
e-mail: carlosmera@itm.edu.co

L. M. Sepúlveda-Cano
Escuela de Administración, EAFIT, Carrera 49 N 7 Sur-50, Medellín 050023, Antioquia, Colombia
e-mail: lmsepulvec@eafit.edu.co

Keywords Foamed concrete · Pore structure · Pore segmentation · Non-specialized images

1 Introduction

Cellular concrete is a type of lightweight concrete. American Institute of Concrete (ACI) in 523 defines lightweight cellular concrete as “a mixture of cement, water, and foam”. The purpose of the foam is to



supply a production mechanism of a high ratio of air cells that, when mixed with cement, produce a porous solid [1, 2]. The main characteristic of cellular concrete is low density, usually between 300 and 1800 kg/m³. In a hardened state, concrete properties such as permeability, shrinkage, thermal conductivity, and mechanical properties are related to porosity, and pore structure [3, 4]. The pore structure is associated with foam stability in a fresh state. The better foam stability generates tiny pores and narrow pore size distribution [5]. Fine and close pores result in a compact texture with high strength, and low permeability [6]. The pores in a foamed concrete might be generated in different configurations: inter-layer (< 1 nm), gel (1 – 10 μm), capillary (> 10 μm), and suction (1 – 2 mm). The larger pores in foamed concrete can be treated as aggregates of zero density. Experimental reports show that foam concrete's pore diameters range between 100 and 200 μm [6, 7]. Water to cement ratio, preparation methods, type of foaming agents, and curing process also affect pore size distribution [8, 9]. The porosity of foamed concrete is measured experimentally by water vacuum saturation or Mercury Intrusion Porosimetry (MIP) methods [10]. However, the experimental porosity measurement is a complicated procedure that may destroy the test specimen. An important issue about experimental porosity determination is that a measure only considers pores where fluid (water, water-steam, or mercury) can arrive. The closed and isolated pore cannot be considered.

Nevertheless, main pore structure characteristics such as pore size distribution, shape descriptors, and spacing are not experimentally measurable. Digital image analysis is an essential tool to determine these parameters. In most cases, specialized images are needed. As some authors report, optical microscopy image processing is the most common technique applied in concretes. Image segmentation was proposed by thresholding the pore size measurement [11]. A similar method was proposed in [6] but using Scanning Electron Microscope (SEM) images. Their main conclusions were that the pore diameters are mainly in the typical range under 200 μm with close and well-distributed pores, representing a compact texture. [12] used SEM images to examine the microstructural characteristics of the foamed concrete with fly ash. The images indicate that, because of the

high amount of foam in the mix, the bubbles were very close to each other, explaining the low compressive strength of foam concrete. Also, [13], using SEM images, showed protein-based foamed concrete has unconnected isolated pores of smaller size, circular with a well-defined boundary compared to synthetic-based. Then, the protein-based foaming agent possesses higher strength and stability than the synthetic foaming agent. X-ray image analysis to determine the porosity of a pervious concrete sample made in the laboratory was evaluated by two approaches: measuring weights and 2D and 3D. Binary images were obtained through Otsu's methodology [14]. The authors use images with a length of 30 mm with 0.5 mm increments.

Other researchers propose the use of tomography [15]. Filtering (erosion-dilation), binarization (thresholding), and correction (Betti numbers) for pore segmentation were used. Each image voxel was classified according to the structure of its neighbors. Subsequently, structuring and individualization were carried out to identify the voxels' structure. Another pore segmentation procedure on 2D or 3D image analysis of void area or volume fraction (average porosity) was reported by [16].

Guo et al. [17], using X-ray computed tomography (X-CT) images, evaluate pore morphology quantitatively. Foamed concrete with different densities has a different porosity and a noticeable difference in pore size distribution. In the same line of analysis, in [2], using threshold images of micro-Computed tomography (micro-CT) in conjunction with probabilistic and quantitative methods was proposed to determine the characteristics of foamed concrete. Other studies report micro-CT image analysis to determine pore structure characteristics and the influence of dosage on performance [18–20]. A combination of upper and lower-scale micro-CT images can provide information on pore and solid characteristics of foamed concrete specimens.

More sophisticated techniques based on 3D representations of foamed concrete samples have also been reported in the literature. In [21], for example, a 3D reconstruction of the cellular concrete was made, aiming to characterize the concrete parameters such as porosity, pore size, and distribution. The authors conducted a methodology including 3D reconstruction with projecting grating and using the RANSAC



algorithm to determine the pore parameters using morphological means.

Although the expected results have been obtained using specialized image processing in the literature, the object's obtention is expensive and has limited access to industrial or massive applications. As experimental porosity determination and specialized image analysis are complex methods, developing an alternative method to understand cellular concretes' porosity has a significant impact. Using non-specialized images is a new way (easy and low cost) to study porosity in foamed concretes.

This work presents a porosity estimation, and pore structure characterization of foamed OPC pastes made with alternative reagents using non-specialized image digital processing. This paper's main goal is to develop a more straightforward and effective method to obtain an estimated value of porosity and pore characteristics using 2D images obtained from a digital camera.

2 Materials and methods

2.1 Materials

Ordinary Portland Cement OPC (equivalent to UG in NTC 121:2021) by Argos Colombia was used to prepare six foamed paste mixes. Alternative foaming agents, conventional air-entraining agents, but in over usual dosage, are used to produce the foam. SikaAer® and AirToc D® were chosen for experimental work due are commercially available around the world. The cement content was kept at 500 kg for each m^3 of the mix in the dosages. The foaming agent was used at 3 wt% respect cement dosage and water to cement ratio W/C in a range of 0.6 – 0.8 to obtain different density samples between 300 and 1000 kg/m^3 . As the reagent is an air-entraining, not a foaming agent, more water is needed to produce stable foam. The manufacturing method of cellular paste was in-mixing, which means that bubbles are formed during mixing cement, water, and reagent. All mixes were made using a HOBART® mixer model N50. A set of trials determined the mixing protocol to evaluate the best mixing time. For this experimental setup, the procedure was: (1) addition of reagent and water with slow addition of cement for 10 minutes at

speed 1; (2) scraping and homogenizing the mixture for 2 minutes and (3) mixing at speed 2 for 8 minutes. The total mixing time was 20 minutes. With foamed pastes, 5 cm edge mortar cubes were melted and wet cured for 28 days. Likewise, measurements of dry density (ASTM C642), porosity (ASTM C642-13), and compressive strength (ASTM C109) were obtained experimentally at 28 days. Experimental characterization results are shown in Table 1. Experimental results show that porosity is strongly related to hardened properties. Compressive strength and density are higher when the porosity is lower, indicating that a closed pore structure results in better mechanical performance. Foaming agent type and water content affect measure porosity. Hardened samples were prepared for obtaining the digital images. Samples were polished to exposed pore features.

2.2 Methods

In this work, we propose a methodology framed in an artificial vision system for the cellular concrete paste samples characterization and porosity estimation. Figure 1 shows the proposed method's scheme, including the following steps: (i) image acquisition, (ii) image pre-processing, (iii) pore segmentation, (iv) feature extraction and porosity estimation.

2.2.1 Image acquisition

Stage in which the capture devices (or sensors) obtain the object's images to be analyzed, which is a cellular concrete sample. Depending on the type of sensor used, the images can be photographs (visible spectrum), X-ray images, gamma-ray images, thermographies, ultrasounds (ultrasound), or range images (3D images), among others.

To standardize the acquisition of images of the cellular concrete samples, an image capture protocol was developed to create the image database required for the subsequent stages of the machine vision system. Specifically, a reflex digital camera was employed with a 50 mm lens, using an aperture of f11. The concrete sample was positioned approximately 50 cm far from the lens, looking to maintain the parallelism between the camera's plane and the sample's one. Also, the camera flash was used, but decreasing its intensity at the minimum (–3.0). The sample was positioned over a black background to

Table 1 Experimental test samples characterization

| Sample | Water-cement ratio | Porosity (%) | Density (%) | Compressive strength (MPa) |
|-------------|--------------------|--------------|-------------|----------------------------|
| AirToc-01-0 | 0.6 | 27 | 1022.91 | 14.81 |
| AirToc-06-0 | 0.7 | 33 | 894.06 | 6.81 |
| AirToc-13-0 | 0.8 | 38 | 704.06 | 6.85 |
| Sika-01-0 | 0.6 | 33 | 1012.07 | 13.76 |
| Sika-13-0 | 0.7 | 39 | 887.13 | 8.07 |
| Sika 25-0 | 0.8 | 44 | 345.5 | 5.38 |

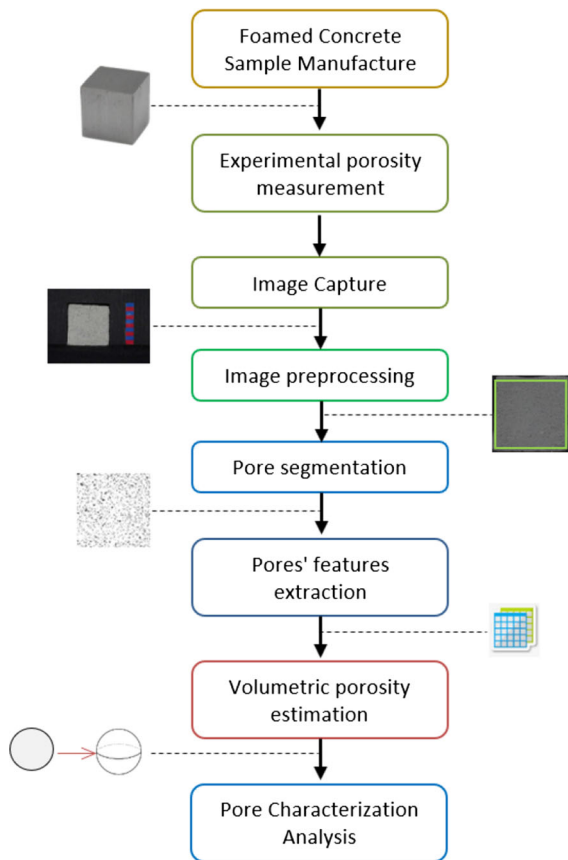


Fig. 1 A proposed methodology for cellular concrete samples characterization

facilitate its segmentation. Furthermore, a 5 mm striped blue/red pattern was placed at the sample’s side to estimate each pixel’s length (mm) at the image, as shown in Fig. 2.

Different from other approaches in the state-of-the-art, in this work, a regular camera was used to capture the pore structure to facilitate replication of the experiments. It will also help develop a mobile phone application to estimate the pore density in a concrete

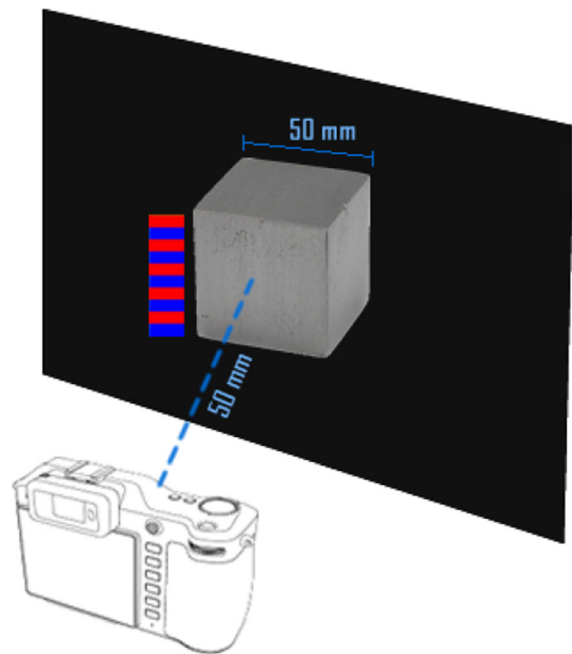


Fig. 2 Capture protocol sketch

Table 2 Information of captured images

| Parameter | Value |
|-----------------|----------------|
| Image size | 4496 × 3000 px |
| Resolution | 300 ppp |
| ISO | 100 |
| Exposition time | 1/50 s |

sample without special equipment. Capture image information is shown in Table 2.

2.2.2 Image pre-processing

After creating the image dataset with the defined capture protocol, they need to be pre-processed to isolate the concrete sample in the image and eliminate the scaling rules. This procedure will allow us to process only the object of interest (the cellular concrete sample) and not the photograph's additional elements. The pre-processing developed also sought to improve the contrast of the pores with the background that contains them.

First, the proposed method transforms the images from color to grayscale, preserving the luminance information [22]. Afterward, the OTSU-threshold [23] algorithm automatically selects a threshold and then binarizes the images. Next, the method looks for the most prominent object in the image, the concrete sample, and uses its coordinates to cut it. Finally, we crop 60 px around the sample to eliminate the noise in the sample's border. This Pre-processing process is shown in Fig. 3.

2.2.3 Pore segmentation

The segmentation process looks to separate the pores in the concrete sample from their background. A well-known approach to perform the pore segmentation is to employ a global thresholding technique [23]. This approach fixes an intensity value (the threshold), which lets the method separates the pores from the background. Despite the simplicity of the solution, it has poor performance because there is little chance to

get a fixed intensity value to separate the pores from the background with images that have been taken under an uncontrolled illumination environment, like the ones in this study. When there are lighting changes, some pores in the image may be brighter than others due to the light and shadows.

Unlike the global thresholding approach, local adaptive thresholding [21] looks for different threshold values for every pixel or local area in the image. In this study, we used the simplest approach for the experiments where the threshold value is calculated as the mean for the local neighborhood of a pixel subtracted by a constant. After the segmentation, we applied some morphological operations to remove tiny objects, make round the pores and increase their size because the thresholding method gets the pores smaller than their original size. Figure 4 shows the segmentation process for the sample AirToc-1.

2.2.4 Pore feature extraction

In order to characterize the segmented pores in the concrete samples, we calculated some morphological features [24]:

- The perimeter, which is calculated by counting the number of pixels around the pore.
- The area, which equals the number of pixels inside the pore.
- The equivalent diameter, which is the diameter (in pixels) of a circle with the same area of the pore. In this way, if the segmentation process joins two

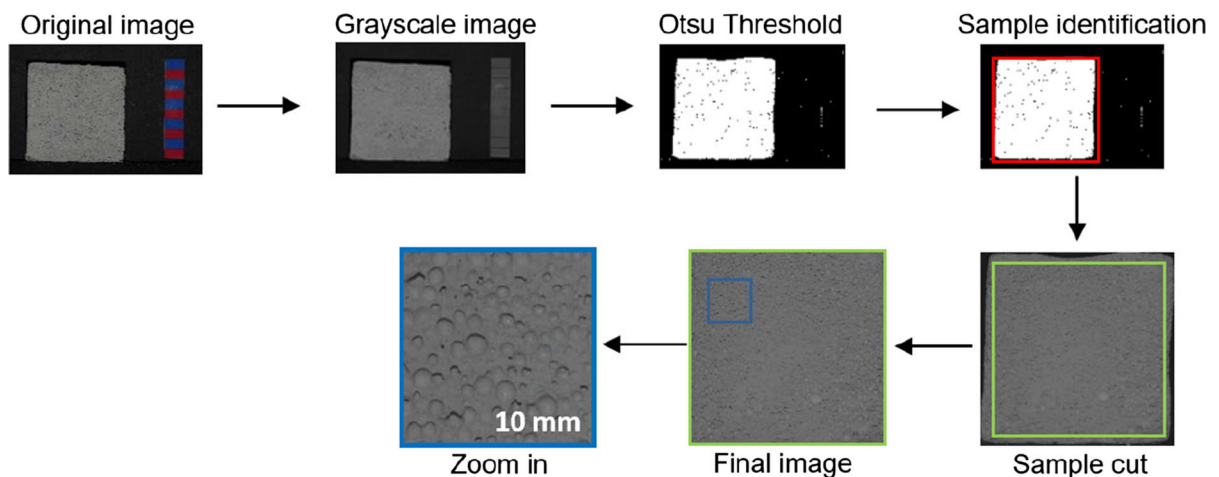


Fig. 3 Pre-processing steps for enhancing the non-specialized images

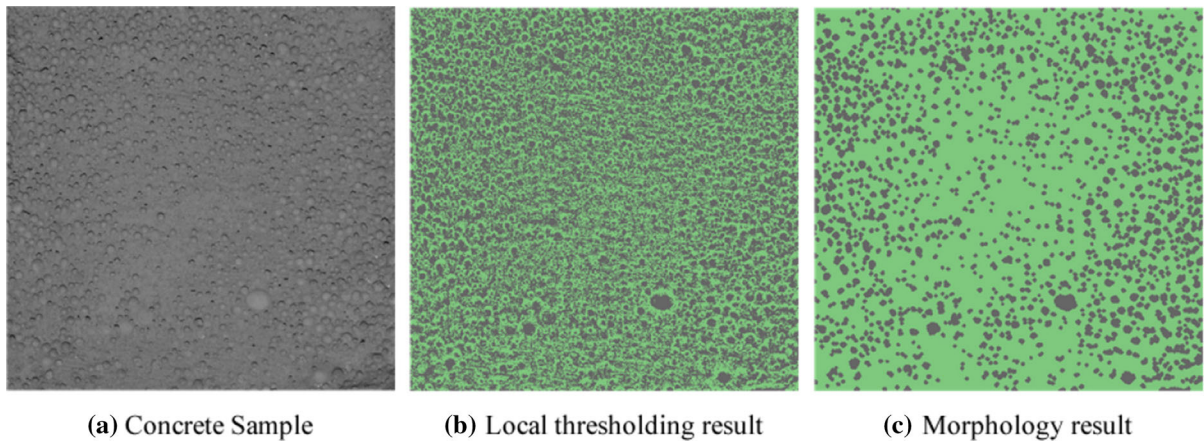


Fig. 4 Pore segmentation process for the sample AirToc-1

pores, the equivalent diameter will represent the diameter of a circular pore with the same number of pixels from the joined pores.

- The solidity, calculated as the ratio between the number of pixels inside the pore and the number of pixels in the convex hull that covers the pore. The convex hull is the smallest convex polygon that surrounds all pixels in the pore.
- Major axis length corresponds to the length of the smallest ellipse’s major axis that fits the pore.
- Minor axis length, which is calculated as the length of the minor axis of the smallest ellipse that fits the pore.

2.2.5 Porosity estimation

To estimate the concrete sample’s porosity, we projected the pore features from the 2D plane to a 3D volume. This process is described below and depicted in Fig. 5.

- First estimated the pores’ diameter in millimeters (mm) using the image’s red and blue patterns. The pattern was isolated by applying a global threshold over the red and blue channels and merging the resulting binary images. After that, the method cuts the second-biggest object in the image, which is the red-blue pattern. Once again, a global threshold and some morphological operators were used over the red and blue channels to separate the blues patterns from the red patterns. Next, the method

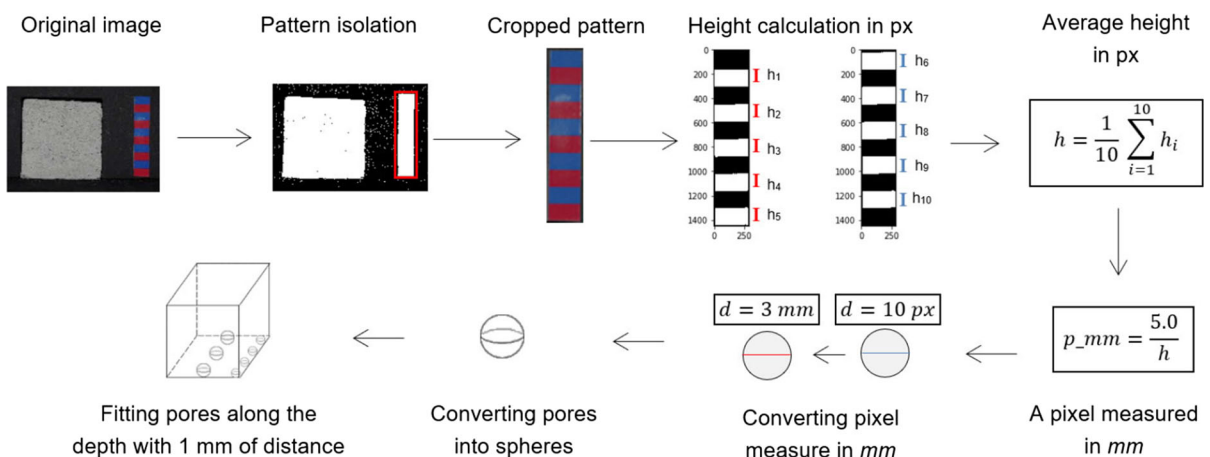


Fig. 5 Volume porosity estimation process



measures the average height in pixels (h) of the blue and red patterns using the equation (1).

$$h = \frac{1}{10} \sum_{i=1}^{10} h_i \quad (1)$$

Then, the measure of a pixel in millimeters (p_mm) is calculated as the ratio $5.0/h$, where 5.0 is the height for each pattern bar in mm. Finally, the pore's diameter in millimeters is calculated as the pore's equivalent diameter multiplied by p_mm .

- Second calculated the volume for each pore. In this step, the 2D pore is converting to a 3D one using its diameter in mm. It was made applying the equation to calculate the volume of a sphere using the pore radius, half of their diameter.
- Third estimated the porosity of a concrete sample based on the volume of their pores. In this step, we assume that the pores' pattern in one side of the cube is repeated throughout its depth. In this way, we projected each pore along with the cube's depth, assuming that each pore is separated in depth from the contiguous one in 1 mm. We add the pores' volume that fits the cube, which is the pores' total volume. After that, we calculated the ratio between total volume pores' and the sample volume, representing the volume porosity estimation. This step is represented by equation (2).

$$volumetric\ porosity = \sum_{i=1}^n [(50 - (60 * 4 * h)/(v_i + 1)] * v_i, \quad (2)$$

where n is the number of pores in the image, 50 is the side of the sample in mm, 60 is the number of pixels that we crop for each side of the cube image, 4 refers to the number cube's sides, 1 is the distance among contiguous pores in mm and v_i is the volume of the pore i .

3 Results

3.1 Pore characterization analysis

Based on the morphological features from the pores, we start analyzing the correlation between variable pairs. Correlation is a measure of how two variables relate to one another. The greater the correlation

coefficient, the more closely related they are. In general, a positive correlation means that the values of two variables move in the same direction; a negative correlation means they move in opposite directions [25]. A useful tool to visualize the correlation among variables is a heat map. Figure 6 shows the correlation among the pores' morphological features using a heat map. High red or blue hues levels represent strong correlations between two parameters. That figure shows that the area, perimeter, major and minor axis length have a strong relationship with equivalent diameter, as we expected. Their lowest correlation coefficient value is 0.82. Volume has no substantial relationship with equivalent diameter due to the map taking a linear correlation. For this reason, it is appropriate to adopt the pore radius and area trend to represent all these parameters. Shape descriptors as solidity and eccentricity have not a high correlation with each other. Their correlation coefficient is 0.67. Changing the trend for shape descriptors implies it is better to consider the shape descriptor analysis separately.

3.1.1 Pore radius distribution and area analysis

Figure 7 shows the pore size and area of samples for AirToc and SikaAer in a box plot. The information extracted from the images indicates that the pore radius increases in samples with lower density and highest porosity. The size pore distribution for each reagent sample is shown in Fig. 8. For AirToc, the finest distribution is from AirToc 01, while most coarse size distribution is from AirToc 13. In Sika samples, the finest distribution is from Sika 01 and coarser from Sika 25. This information corresponds with the box plot as well. In this study, Sika 25 is the specimen with lower density, and the pore size is between 0.1 and 1.3 mm. Besides, AirToc 01 has the highest density and lower porosity. The pores size range for this sample is between 0.1 and 0.9 mm. As the pore area has a strong correlation with the diameter (or radius), the same tendency occurs in samples. While lower density, the area has a higher value.

For best pore size analysis, pores have been divided by size into four categories as suggested on [9]: gel or interlayer ($< 10\text{ nm}$); macrocapillary ($> 10\text{ }\mu\text{m}$); suction ($1 - 2\text{ mm}$) and macropores $> 2\text{ mm}$. Figure 9 shows a plot as number distribution and percentage of the occupied area by pore category, divided by

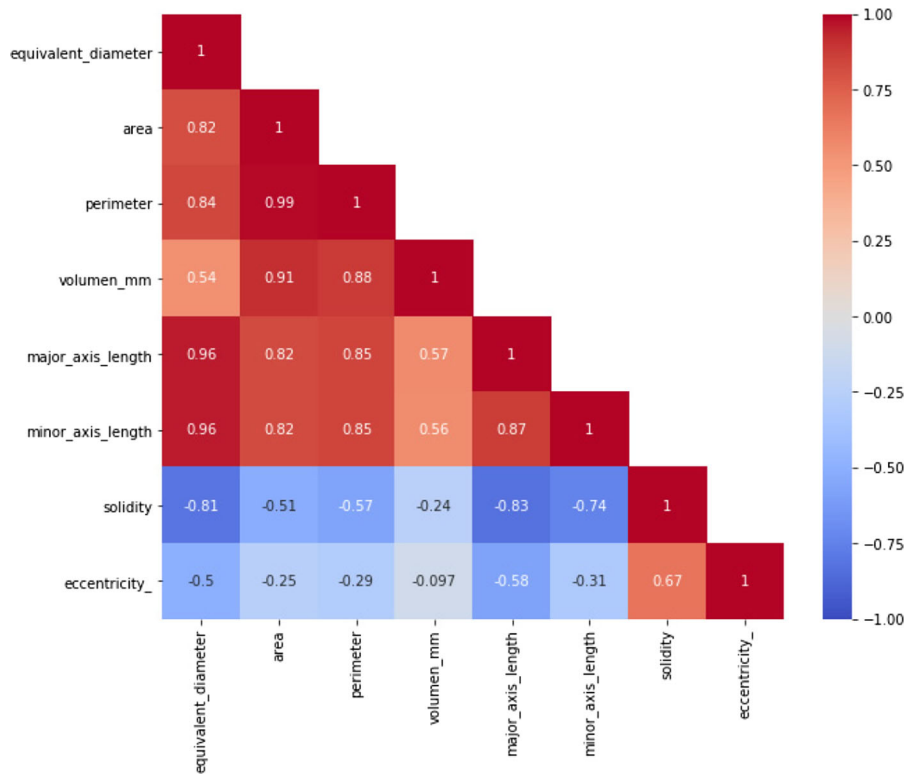


Fig. 6 Heatmap of features correlation result

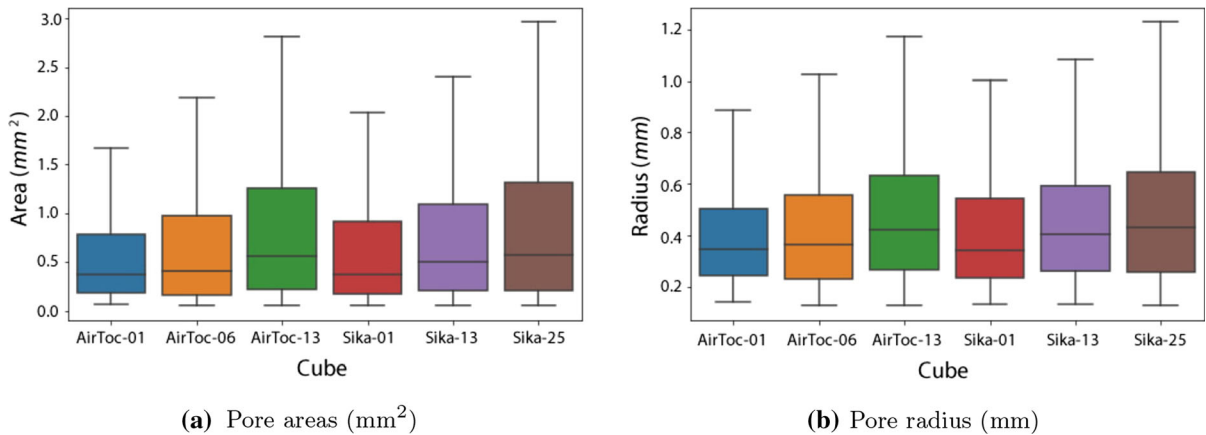


Fig. 7 Pore box charts for the a area and b radius for each concrete sample

reagent. Results reveal that pore structure is strongly connected with total porosity in the sample. Table 3 presents data about pore numbers obtained by image analysis.

For Sika, the number of capillary pores is strongly dominant in all samples. However, when density decreasing the number of macropores and suction

pores increases, begin to have greater relevance in the porous structure. Results show clearly that macropores are in lower quantity. However, they fill a big part of the total area, in contrast to the low area occupied by a significant number of capillary pores (see Fig. 9a). However, in all Sika samples, suction pores provide the major percentage of area occupation. A similar



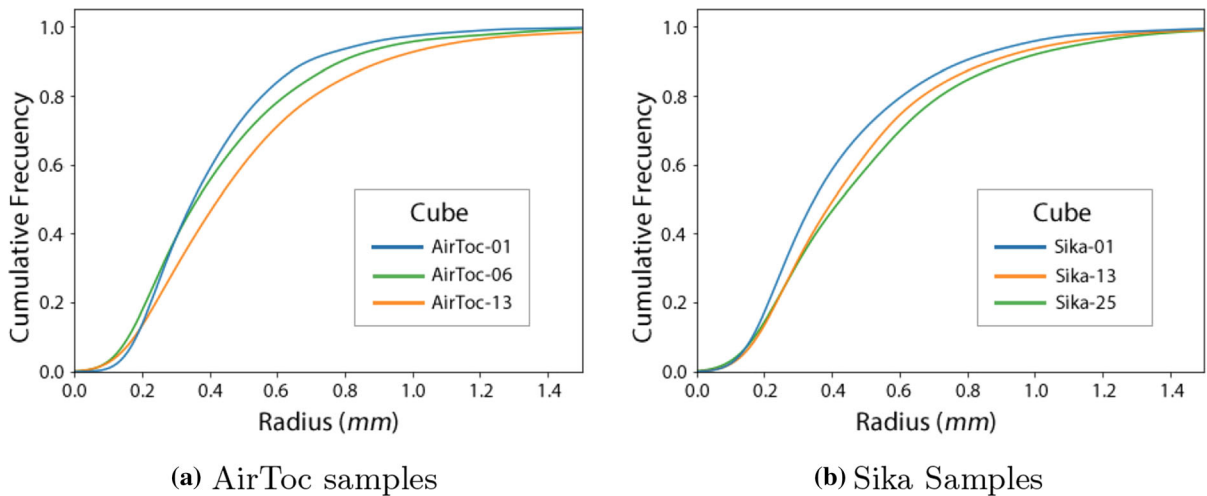


Fig. 8 Cumulative frequency of equivalent radius for AirToc and Sika samples

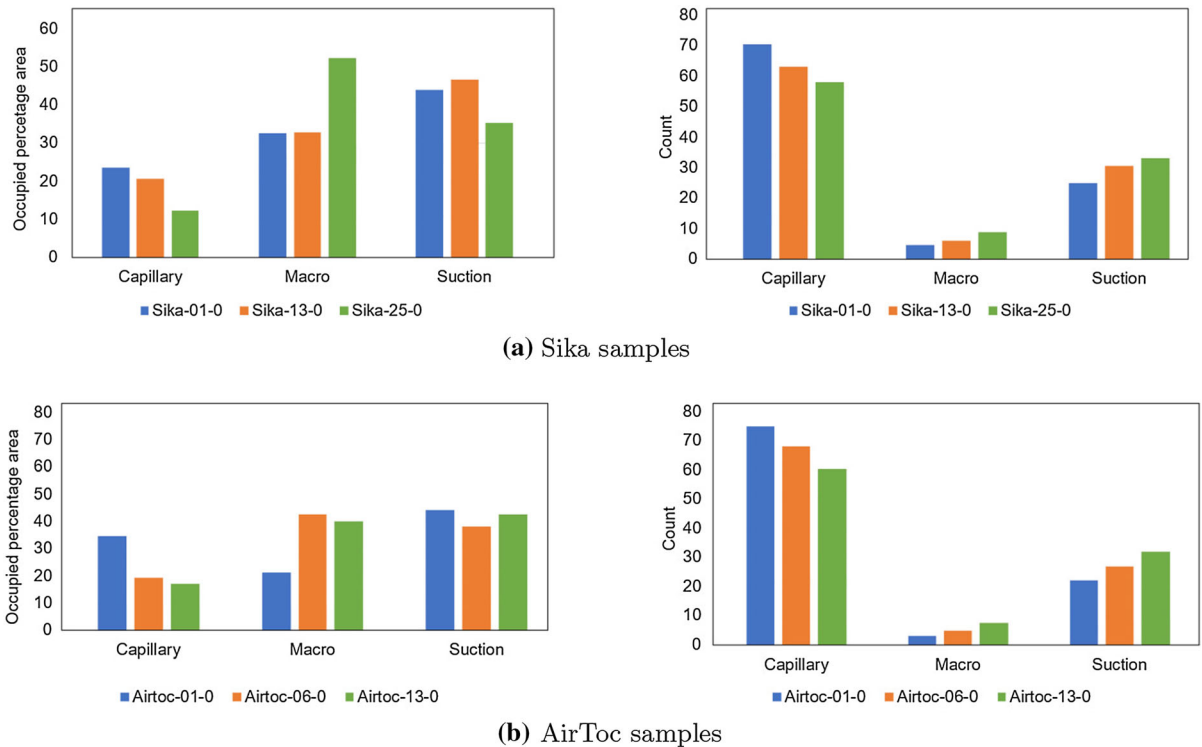


Fig. 9 Comparison between pore number and percentage of the occupied area by reagent

trend occurs when analyzing pore structure from AirToc samples. The main difference is that all types of pores have almost the same magnitude of the filled area percentage. In general, the less dense the sample, the smaller the total number of pores present.

3.1.2 Shape descriptors analysis

Figure 10 shows a box plot for shape descriptors and Table 4 shows the results for the average value of the features calculated by pore type. In general, capillaries pores tend to be more spherical because their



Table 3 Pore number and pore occupation by area

| Sample | Pore count | Area filled by pores (%) | Pore type | Pore area by type (%) | Pore count by type (%) |
|-----------|------------|--------------------------|-----------|-----------------------|------------------------|
| AirToc-01 | 1204 | 43.7 | Capillary | 34.5 | 74.9 |
| | | | Macro | 21.3 | 2.9 |
| | | | Suction | 44.2 | 22.2 |
| AirToc-06 | 1060 | 52.5 | Capillary | 19.20 | 68.2 |
| | | | Macro | 42.3 | 4.9 |
| | | | Suction | 38.2 | 26.9 |
| AirToc-13 | 1107 | 59.9 | Capillary | 17.2 | 60.4 |
| | | | Macro | 40.2 | 7.5 |
| | | | Suction | 42.6 | 32.1 |
| Sika-01 | 1160 | 52.7 | Capillary | 23.6 | 70.60 |
| | | | Macro | 32.5 | 4.5 |
| | | | Suction | 43.9 | 24.9 |
| Sika-13 | 1154 | 56.4 | Capillary | 20.7 | 63.3 |
| | | | Macro | 32.8 | 6.1 |
| | | | Suction | 46.6 | 30.7 |
| Sika-25 | 897 | 65.1 | Capillary | 12.3 | 58.1 |
| | | | Macro | 52.4 | 8.7 |
| | | | Suction | 35.3 | 33.2 |

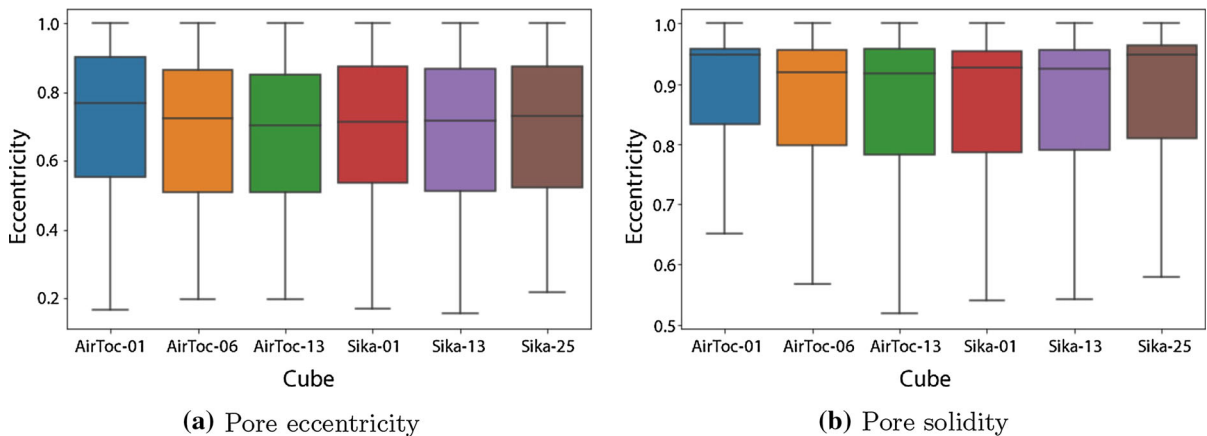


Fig. 10 Pore box charts for the **a** eccentricity and **b** solidity for each concrete sample

eccentricity is closer to 1. The difference in length between the major and minor axis is the smallest. The capillaries pore also have the highest solidity which means that they are geometrically denser. Macropores are the most eccentric because of the more significant difference between their axes' length. Regarding sphericity, macropores tend to be less solid as consequence of bleeding or coalescence on bubbles.

A relevant aspect is that as the density decreases, the solidity of each type of pore increases. This shows the effect of dosing on the porous structure.

3.2 Volumetric porosity estimation from images

From the analysis of non-specialized images, the volume occupied by the pores was estimated. As



Table 4 Average of the features calculated over the pores in the concrete samples according the pore type

| Sample | Pore type | Eccentricity | Major axis (px) | Minor axis (px) | Solidity |
|-----------|-----------|--------------|---------------------|---------------------|----------|
| AirToc-01 | Capilar | 0.71 | 19.36 | 13.80 | 0.93 |
| | Macro | 0.52 | 118.65 | 61.76 | 0.58 |
| | Suction | 0.55 | 51.84 | 28.48 | 0.79 |
| AirToc-06 | Capilar | 0.69 | 21.45 | 14.76 | 0.92 |
| | Macro | 0.47 | 151.20 | 71.07 | 0.57 |
| | Suction | 0.51 | 64.70 | 32.79 | 0.77 |
| AirToc-13 | Capilar | 0.72 | 22.02 | 15.79 | 0.94 |
| | Macro | 0.47 | 146.42 | 68.58 | 0.61 |
| | Suction | 0.50 | 65.29 | 32.91 | 0.77 |
| Sika-01 | Capilar | 0.70 | 20.03 | 13.92 | 0.92 |
| | Macro | 0.48 | 135.85 | 64.62 | 0.58 |
| | Suction | 0.53 | 61.91 | 32.60 | 0.74 |
| Sika-13 | Capilar | 0.71 | 20.84 | 14.78 | 0.93 |
| | Macro | 0.41 | 146.06 | 59.82 | 0.60 |
| | Suction | 0.53 | 59.51 | 31.32 | 0.78 |
| Sika-25 | Capilar | 0.73 | 21.05 | 15.30 | 0.94 |
| | Macro | 0.42 | 146.86 | 61.79 | 0.64 |
| | Suction | 0.55 | 60.63 | 33.53 | 0.82 |

indicated in Sect. 2, the procedure consisted of estimating the area occupied by pores in a section; this is in a non-specialized flat image of the sample. The volumetric projection (volume occupied by the pores) is performed considering a layer thickness defined by the diameter of the largest pore present in the analyzed layer. The results, presented in Table 5, show that it is possible to estimate porosity through the previous procedure. The estimation error is negligible (1%) for samples manufactured with AirToc. In the case of Sika test pieces, the maximum error value is less than 10%. The difference between the two deviations on porosity estimation it should be due the difference on pore structure for each reagent. Also,

the interconnection between pores-that it can not detected in 2D image- maybe can affect porosity estimation. However, if it considers that the analyzed images can be obtained easily following the established protocol of capture and with a very low error in the estimation regarding the porosity obtained experimentally, this procedure can be implemented at the industrial level.

4 Conclusions

Using 2D non-specialized images is a more straightforward and effective way to obtain porosity

Table 5 Volumetric porosity estimated using the proposed methodology

| Sample | Sample volume (mm^3) | Pore volume (mm^3) | Volumetric porosity (%) | Experimental porosity (%) |
|-------------|---------------------------------|-------------------------------|-------------------------|---------------------------|
| AirToc-01-0 | 87376.95 | 23384.03 | 26.76 | 27.0 |
| AirToc-06-0 | 96886.77 | 31812.49 | 32.83 | 33.0 |
| AirToc-13-0 | 97605.26 | 36511.48 | 37.40 | 38.0 |
| Sika-01-0 | 86816.13 | 28317.70 | 32.62 | 33.0 |
| Sika-13-0 | 91822.96 | 32151.25 | 35.01 | 39.0 |
| Sika 25-0 | 91096.58 | 37456.62 | 41.10 | 44.0 |

estimation and pore structure characterization. The main issue relates to image acquisition protocols for foamed OPC pastes using a regular digital camera. The proposed methodology isolates the pores in a 2D image and measures some shape features. The diameter measured in pixels is translated into millimeters and then used to project each pore into a volumetric shape, assuming that a sphere represents volume. The proposed method permits a rough estimation of porosity. Porosity was calculated as the ratio between the pores' volume and the total concrete sample volume. The volumetric projection (volume occupied by the pores) is performed considering a layer thickness defined by the diameter of the largest pore in the analyzed layer. Differences between experimental and estimated porosity by digital image analysis were under 10%, indicating the proposed method is accurate enough. Due to the image's nature, this method can be extended easily on an industrial level.

Regarding pore structure related to samples made with alternative reagents, results show that porosity estimation has a deviation of less than 1% in AirToc® samples and less than 10% in SikaAer® samples. Pore diameter obtained in millimeters permits classification into capillary, suction, and macropore classes. Pore analysis shows that pore size distribution, shape, and area occupation are related to the foaming agent. Close pore structure results in better mechanical performance.

Author Contributions All authors contributed to the study conception and design, material preparation, data collection and analysis. All authors read and approved the final manuscript.

Funding Open Access funding provided by Colombia Consortium. The authors would like to thank the Universidad de Medellín and the Instituto Tecnológico Metropolitano de Medellín - ITM, for financing the project with codes UdeM-1067 and ITM-PE19110, respectively.

Declarations

Conflict of interest The authors have no relevant financial or non-financial interests to disclose.

Open Access This article is licensed under a Creative Commons Attribution 4.0 International License, which permits use, sharing, adaptation, distribution and reproduction in any medium or format, as long as you give appropriate credit to the original author(s) and the source, provide a link to the

Creative Commons licence, and indicate if changes were made. The images or other third party material in this article are included in the article's Creative Commons licence, unless indicated otherwise in a credit line to the material. If material is not included in the article's Creative Commons licence and your intended use is not permitted by statutory regulation or exceeds the permitted use, you will need to obtain permission directly from the copyright holder. To view a copy of this licence, visit <http://creativecommons.org/licenses/by/4.0/>.

References

- Gomez M (2015) An introduction to cellular concrete & advanced engineered foam technology. In: 2015 engineering and construction exchange
- Chung S-Y, Lehman C, Abda Elrahman M, Stephan D (2017) Pore characteristics and their effects on the material properties of foamed concrete evaluated using micro-ct images and numerical approaches. *Appl Sci* 7(6):550. <https://doi.org/10.3390/app7060550>
- Narayanan N, Ramamurthy K (2000) Structure and properties of aerated concrete: a review. *Cem Concr Compos* 22(5):321–329. [https://doi.org/10.1016/S0958-9465\(00\)00016-0](https://doi.org/10.1016/S0958-9465(00)00016-0)
- Feneuil B, Roussel N, Pitois O (2019) Optimal cement paste yield stress for the production of stable cement foams. *Cem Concr Res* 120:142–151. <https://doi.org/10.1016/j.cemconres.2019.03.002>
- He J, Gao Q, Song X, Bu X, He J (2019) Effect of foaming agent on physical and mechanical properties of alkali-activated slag foamed concrete. *Constr Build Mater* 226:280–287. <https://doi.org/10.1016/j.conbuildmat.2019.07.302>
- Yu XG, Luo SS, Gao YN, Wang HF, Li YX, Wei YR, Wang XJ (2010) Pore structure and microstructure of foam concrete. *Adv Mater Res* 177:530–532. <https://doi.org/10.4028/www.scientific.net/AMR.177.530>
- Kearsley EP, Wainwright PJ (2001) Porosity and permeability of foamed concrete. *Cem Concr Res* 31(5):805–812. [https://doi.org/10.1016/S0008-8846\(01\)00490-2](https://doi.org/10.1016/S0008-8846(01)00490-2)
- Li Y, Dong W, Li H, Li Z (2019) Method of vacuum water absorption to determine the porosity of hardened concrete. *Int J Struct Civil Eng Res* 4(3):282–286. <https://doi.org/10.18178/ijscer.4.3.282-286>
- Chica L, Alzate A (2019) Cellular concrete review: new trends for application in construction. *Constr Build Mater* 200:637–647. <https://doi.org/10.1016/J.CONBUILDMAT.2019.03.270>
- Amran Y, Farzadnia N, Abang Ali A (2015) Properties and applications of foamed concrete; a review. *Constr Build Mater* 101:990–1005. <https://doi.org/10.1016/j.conbuildmat.2015.10.112>
- Nambiar EKK, Ramamurthy K (2006) Influence of filler type on the properties of foam concrete. *Cem Concr Compos* 28(5):475–480. <https://doi.org/10.1016/j.cemconcomp.2005.12.001>
- Abd Elrahman M, El Madawy ME, Chung S-Y, Sikora P, Stephan D (2019) Preparation and characterization of ultra-lightweight foamed concrete incorporating lightweight



- aggregates. *Appl Sci* 9(7):1447. <https://doi.org/10.3390/app9071447>
13. Hashim M, Tantray M (2021) Comparative study on the performance of protein and synthetic-based foaming agents used in foamed concrete. *Case Stud Constr Mater* 14:00524. <https://doi.org/10.1016/j.cscm.2021.e00524>
 14. Ahn J, Jung J, Kim S, Han S-I (2014) X-ray image analysis of porosity of pervious concretes. *Int J GEOMATE Geotech Constr Mater Environ* 6(1):796–799
 15. Almhdie A, Rozenbaum O, Lespessailles E, Jennane R (2014) Image processing for the non-destructive characterization of porous media. application to limestones and trabecular bones. *Mathematics and Computers in Simulation* 99, 82–94 . <https://doi.org/10.1016/j.matcom.2013.07.003>. In: MAMERN IV–2011: The 4th International Conference on Approximation Methods and Numerical Modeling in Environment and Natural Resources- PART I
 16. Du Plessis A, Olawuyi BJ, Boshoff WP, Le Roux SG (2016) Simple and fast porosity analysis of concrete using x-ray computed tomography. *Mater Struct* 49(1–2):553–562
 17. Guo Y, Chen X, Chen B, Wen R, Wu P (2021) Analysis of foamed concrete pore structure of railway roadbed based on x-ray computed tomography. *Constr Build Mater* 273:121773. <https://doi.org/10.1016/j.conbuildmat.2020.121773>
 18. Chung S-Y, Lehmann C, Abd Elrahman M, Stephan D (2017) Pore characteristics and their effects on the material properties of foamed concrete evaluated using micro-ct images and numerical approaches. *Appl Sci* 7(6):550. <https://doi.org/10.3390/app7060550>
 19. Elrahman MA, Sikora P, Chung S-Y, Stephan D (2021) The performance of ultra-lightweight foamed concrete incorporating nanosilica. *Arch Civil Mech Eng* 21:79. <https://doi.org/10.1007/s43452-021-00234-2>
 20. Chung S-Y, Kim J-S, Han T-S, Stephan D, Kamm PH, Elrahman MA (2022) Characterization of foamed concrete with different additives using multi-scale micro-computed tomography. *Constr Build Mater* 319:125953. <https://doi.org/10.1016/j.conbuildmat.2021.125953>
 21. Roy P, Dutta S, Dey N, Dey G, Chakraborty S, Ray R (2014) Adaptive thresholding: A comparative study. In: 2014 International Conference on Control, Instrumentation, Communication and Computational Technologies (ICCICT), pp. 1182–1186 . <https://doi.org/10.1109/ICCICT.2014.6993140>
 22. Burger W, Burge MJ (2009) Principles of digital image processing. Springer, London. <https://doi.org/10.1007/978-1-84800-195-4>
 23. Sezgin M, Sankur B (2004) Survey over image thresholding techniques and quantitative performance evaluation. *J Electron Imaging* 13(1):146–165. <https://doi.org/10.1117/1.1631315>
 24. Nixon MS, Aguado AS (2019) Feature extraction and image processing for computer vision. Academic Press, Cambridge. <https://doi.org/10.1016/C2017-0-02153-5>
 25. Kowalski CJ (1972) On the effects of non-normality on the distribution of the sample product-moment correlation coefficient. *J Royal Stat Soc Ser C Appl Stat* 21(1):1–12

Publisher's Note Springer Nature remains neutral with regard to jurisdictional claims in published maps and institutional affiliations.

